

Functional Horseshoe Smoothing for Functional Trend Estimation

Tomoya Wakayama^{*1} and Shonosuke Sugasawa[†]

^{*}Graduate School of Economics, The University of Tokyo

[†]Center for Spatial Information Science, The University of Tokyo

Abstract

Due to developments in instruments and computers, functional observations are increasingly popular. However, effective methodologies for flexibly estimating the underlying trends with valid uncertainty quantification for a sequence of functional data (e.g. functional time series) are still scarce. In this work, we develop a locally adaptive smoothing method, called functional horseshoe smoothing, by introducing a shrinkage prior to the general order of differences of functional variables. This allows us to capture abrupt changes by taking advantage of the shrinkage capability and also to assess uncertainty by Bayesian inference. The fully Bayesian framework also allows the selection of the number of basis functions via the posterior predictive loss. Also, by taking advantage of the nature of functional data, this method is able to handle heterogeneously observed data without data augmentation. We show the theoretical properties of the proposed prior distribution and the posterior mean, and finally demonstrate them through simulation studies and applications to a real-world dataset.

Keywords: functional time series; shrinkage prior; Markov chain Monte Carlo; tail robustness; trend filtering

¹Corresponding author, Email: tom-w9@g.ecc.u-tokyo.ac.jp

1 Introduction

Owing to the remarkable development of measuring instruments and computers in recent years, it has become possible to obtain high-dimensional data in various fields. On the other hand, the analysis of such data using classical multivariate analysis requires a huge number of parameters, which is an obstacle in extracting valuable information from the data. A promising methodology to solve these problems is functional data analysis (FDA), which treats and analyzes high-dimensional data as a curve (function). Functional versions for many branches of statistics have been provided such as Ramsay (2004), Kokoszka and Reimherr (2017), and Horváth and Kokoszka (2012), and it is a field that has been the focus of much research.

The traditional FDA approach for independent functional data has recently been extended to time series. In fact, for functional time series data, the standard stationary model for multivariate data has been extended (e.g. Besse et al., 2000; Klepsch and Klüppelberg, 2017; Klepsch et al., 2017; Hörmann et al., 2013; Gao et al., 2019; Hörmann et al., 2015) and its theoretical properties have been extensively studied (e.g. Bosq, 2000; Aue and Klepsch, 2017; Spangenberg, 2013; Aue et al., 2017; Kühnert et al., 2020; Cerovecki et al., 2019). However, in actual data such as GDP, the assumption of stationarity is not satisfied in many situations because the expected value varies from period to period. There are a few cases where the trend can be analyzed appropriately by existing methods.

Due to the stationarity of conventional FDA methods, they cannot capture rapid changes in trend estimation, but Wakayama and Sugawara (2021) solved this difficulty by developing a new type of lasso and proposing functional trend filtering. This new method can capture local changes while removing observation errors in the data. In other words, the method can clearly identify when structural changes occur in time series data. In order for the inferred results to be used for decision-making, it is essential to evaluate the interpretability of the model and the uncertainty of the prediction. However, few methods for uncertainty evaluation in functional time series analysis have been developed (Petrís, 2013; Canale and Ruggiero, 2016).

In this work, we develop the other approach in a Bayesian framework, hoping to assess uncertainty and estimate trend accurately and flexibly as seen in univariate models (Faulkner and Minin, 2018). In the context of FDA, a shrinkage prior on the functional space has been introduced by Shin et al. (2020). Utilizing a similar idea, we construct a locally adaptive smoother for functional data via the shrinkage prior. Because the priors in the model can be represented as scale mixture of normals, it is easy to implement with the Gibbs sampler, and minor extensions make heterogeneously observed data analysis possible. We derive posterior predictive loss based on Gelfand and Ghosh (1998) to choose an appropriate number of basis functions.

We also discuss the theoretical justification for this approach. The essence of this method is that it removes noise while leaving the change points large. The property of the prior that keeps the signal from shrinking is called "tail robustness". We show that the method achieves this property due to a heavy-tail prior. This is not an argument closed to functional data, but also justifies a locally adaptive method for finite-dimensional data (Faulkner and Minin, 2018; Kakikawa et al., 2022).

The remainder of the paper is structured as follows. Section 2.1 introduces the setting and model for trend estimation. Section 2.2 gives the posterior computation algorithm. In Section 2.3, we present the way to select the number of basis. Section 2.4 discusses the theoretical properties of the proposed prior and its posterior distribution. In Section 3, we investigate the performance of the proposed methods for homogeneously observed data and heterogeneously observed data. We apply our method to a real dataset in Section 4. The contribution of the article is discussed in Section 5.

2 Functional Horseshoe Smoothing

2.1 Settings and models

Let $Y_1(\cdot), \dots, Y_T(\cdot)$ be observed functional data on $\mathcal{S} \subset \mathbb{R}$, ordered as $t = 1, \dots, T$. Suppose that we are interested in the mean function $Z_t(\cdot) \equiv \mathbb{E}[Y_t(\cdot)]$ that may change smoothly or abruptly over t . To estimate Z_t , we employ the following measurement

error model:

$$Y_t(s) = Z_t(s) + \varepsilon_t(s), \quad \varepsilon_t(s) \sim N(0, \sigma^2), \quad t = 1, \dots, T, \quad s \in \mathcal{S},$$

where $\varepsilon_t(s)$ are error terms independent over different values of t and s , and σ^2 is an unknown variance. Such measurement models are adopted in the context of Bayesian modeling of functional data (Yang et al., 2016, 2017).

Let $\phi_1(\cdot), \dots, \phi_L(\cdot)$ be basis functions on \mathcal{S} (e.g. B-spline function) common over t . We model $Z_t(\cdot)$ as

$$Z_t(\cdot) = \sum_{\ell=1}^L b_{t\ell} \phi_\ell(\cdot), \quad t = 1, \dots, T,$$

where $\mathbf{b}_t = (b_{t1}, \dots, b_{tL})^\top$ is a vector of coefficients, and L is the number of basis functions. Thus, heterogeneity of the mean function $Z_t(s)$ is characterized by the heterogeneous coefficients, \mathbf{b}_t . The choice of L controls the smoothness of the estimates of $Z_t(\cdot)$, and we later discuss a data-dependent selection of L .

Let $Y_t(s_{t1}), \dots, Y_t(s_{tn_t})$ be discrete observations, where the s_{t1}, \dots, s_{tn_t} are the observation points and n_t is the number of discrete observations. Note that we allow the number of sampling points and the sampled locations to be heterogeneous over t . Under the settings described above, the model for $\mathbf{y}_t = (Y_t(s_{t1}), \dots, Y_t(s_{tn_t}))^\top$ is

$$\mathbf{y}_t = \Phi_t \mathbf{b}_t + \boldsymbol{\varepsilon}_t, \quad \boldsymbol{\varepsilon}_t \sim N(\mathbf{0}, \sigma^2 I_{n_t}), \quad t = 1, \dots, T,$$

where Φ_t is a $n_t \times L$ matrix whose (i, ℓ) -element is $\phi_\ell(s_{ti})$.

Now, we consider prior distributions on \mathbf{b}_t . Let Δ_k be k th order forward difference operators defined as

$$\Delta_k = \begin{cases} D^{(0)} & \text{for } k = 0, \\ D^{(k)} \Delta_{k-1} & \text{for } k \geq 1, \end{cases}$$

where $D^{(k)}$ is the following $(T - k - 1) \times (T - k)$ matrix:

$$D^{(k)} = \begin{pmatrix} 1 & -1 & 0 & \dots & 0 & 0 \\ 0 & 1 & -1 & \dots & 0 & 0 \\ \vdots & \vdots & \vdots & \ddots & \vdots & \vdots \\ 0 & 0 & 0 & \dots & 1 & -1 \end{pmatrix}.$$

We then define $(\boldsymbol{\delta}_1, \dots, \boldsymbol{\delta}_{T-k-1})^\top = \Delta_k(\mathbf{b}_1, \dots, \mathbf{b}_T)^\top$ and consider a model for this. For example, if $k = 0$, each $\boldsymbol{\delta}_t$ can be written as $\boldsymbol{\delta}_t = \mathbf{b}_{t+1} - \mathbf{b}_t$, for $t = 1, \dots, T - 1$. Hence, if the vector $\boldsymbol{\delta}_t$ is shrunk toward the origin, the two adjacent coefficient vector \mathbf{b}_{t+1} and \mathbf{b}_t are identical, leading to the same mean functions for $Z_t(\cdot)$ and $Z_{t+1}(\cdot)$. To encourage such structures, we introduce shrinkage priors on $\boldsymbol{\delta}_t$, which has a large mass around the origin, whereas the tail of the prior is sufficiently large to allow possible abrupt changes over t . Note that under general k , shrinking $\boldsymbol{\delta}_t$ toward the origin can be regarded as the smoothing of k th order derivatives of $Z_t(\cdot)$ with respect to t . We introduce the following hierarchical prior for $\boldsymbol{\delta}_t$:

$$\boldsymbol{\delta}_t | \lambda_t, \tau, \sigma \sim N(\mathbf{0}, \sigma^2 \tau^2 \lambda_t^2 (\Phi_t^\top \Phi_t)^{-1}), \quad \lambda_t \sim C^+(0, 1), \quad \tau \sim C^+(0, 1), \quad (1)$$

where $C^+(0, 1)$ denotes the standard half-Cauchy distribution. The conditional prior of $\boldsymbol{\delta}_t$ has a form of g -prior (Zellner, 1986), and a hierarchical prior similar to (1) is adopted in Shin et al. (2020) in the context of linear regression models. Here λ_t is a local shrinkage parameter that controls the amount of shrinkage, and λ_t is common to all components of $\boldsymbol{\delta}_t$ so that the vector $\boldsymbol{\delta}_t$ can be simultaneously shrunk toward the origin. The use of the half-Cauchy for the local parameter λ_t leads to a multivariate horseshoe-like prior for $\boldsymbol{\delta}_t$. The prior distribution has favorable properties, given in Section 2.4, and we make the most of them to handle sparsity.

2.2 Posterior computation algorithm

The joint posterior distribution is given by

$$\pi(\sigma^2)\pi(\tau^2)\prod_{t=1}^T\phi(\mathbf{y}_t;\Phi_t\mathbf{b}_t,\sigma^2I_n)\prod_{t=1}^{T-k-1}\phi(\boldsymbol{\delta}_t;\mathbf{0},\sigma^2\tau^2\lambda_t^2(\Phi_t^\top\Phi_t)^{-1})\pi(\lambda_t),$$

where $\pi(\sigma^2)$, $\pi(\tau^2)$ and $\pi(\lambda_t)$ are prior distributions for σ^2 , τ^2 and λ_t^2 , respectively. The priors of τ^2 and λ_t^2 are defined in (1), and we use the conjugate prior, $\sigma^2 \sim \text{IG}(a_\sigma, b_\sigma)$ given hyperparameters a_σ and b_σ . Using the data augmentation technique of the horseshoe prior (e.g. Makalic and Schmidt, 2015), sampling from the joint posterior can be carried out by a simple Gibbs sampling described as follows:

- (Sampling from σ^2) The full conditional distribution of σ^2 is $\text{IG}(\tilde{a}_\sigma, \tilde{b}_\sigma)$, where

$$\begin{aligned}\tilde{a}_\sigma &= a_\sigma + \frac{1}{2}L(T-k-1) + \frac{1}{2}nT, \\ \tilde{b}_\sigma &= b_\sigma + \frac{1}{2}\sum_{t=1}^T(\mathbf{y}_t - \Phi_t\mathbf{b}_t)^\top(\mathbf{y}_t - \Phi_t\mathbf{b}_t) + \frac{1}{2\tau^2}\sum_{t=1}^{T-k-1}\frac{\boldsymbol{\delta}_t^\top\Phi_t^\top\Phi_t\boldsymbol{\delta}_t}{\lambda_t^2}.\end{aligned}$$

- (Sampling from τ^2) The full conditional distribution of τ^2 is

$$\text{IG}\left(\frac{L(T-k-1)+1}{2}, \frac{1}{\xi} + \sum_{t=1}^{T-k-1}\frac{\boldsymbol{\delta}_t^\top\Phi_t^\top\Phi_t\boldsymbol{\delta}_t}{2\sigma^2\lambda_t^2}\right),$$

where ξ is an auxiliary variable whose full conditional distribution is $\text{IG}(1, 1 + 1/\tau^2)$.

- (Sampling from λ_t^2) The full conditional distribution of λ_t^2 is

$$\text{IG}\left(\frac{L+1}{2}, \frac{1}{\nu_t} + \frac{\boldsymbol{\delta}_t^\top\Phi_t^\top\Phi_t\boldsymbol{\delta}_t}{2\tau^2\sigma^2}\right),$$

where ν_t is an auxiliary variable whose full conditional distribution is $\text{IG}(1, 1 + 1/\lambda_t^2)$.

- (Sampling from \mathbf{b}_t) The full conditional distribution of \mathbf{b}_t is of the form, $N(\boldsymbol{\mu}_t, c_t(\Phi_t^\top\Phi_t)^{-1})$, where the specific forms of $\boldsymbol{\mu}_t$ and c_t are dependent on k , the order of difference.

The detailed expressions under $k = 0$ and $k = 1$ in the Appendix 1.

As shown above, all the full conditional distributions are familiar forms; thereby

the posterior computation can be efficiently carried out. Given the posterior samples of \mathbf{b}_t , the posterior samples of $Z_t(s)$ at arbitrary location $s \in \mathcal{S}$ can be generated, which gives point estimate (e.g. posterior mean) and interval estimation (e.g. 95% credible interval).

2.3 Selection of the number of basis functions

In practice, the specification of the number of basis functions, L , is an important task. If L is smaller than necessary, the basis function approximation gives over-smoothed results. On the other hand, the estimation results can be inefficient if L is larger than necessary. We suggest adopting a model selection criterion to select L in a data dependent manner. We here use posterior predictive loss (PPL) proposed by Gelfand and Ghosh (1998).

To clarify the number of basis used in the estimation, we write $\mathbf{b}_t(L)$ and $\Phi_t(L)$ rather than \mathbf{b}_t and Φ_t . Given $\mathbf{b}_t(L)$, the conditional distribution of \mathbf{y}_t is $N(\Phi_t(L)\mathbf{b}_t(L), \sigma^2 I_n)$. We then define the PPL as

$$\begin{aligned} \text{PPL}(L) = & \frac{T}{T+1} \sum_{t=1}^T \{\mathbf{y}_t - \Phi_t(L)\mathbf{E}_p[\mathbf{b}_t(L)]\}^\top \{\mathbf{y}_t - \Phi_t(L)\mathbf{E}_p[\mathbf{b}_t(L)]\} \\ & + nT\mathbf{E}_p[\sigma^2] + \sum_{t=1}^T \text{tr}(\Phi_t(L)\text{Cov}_p(\mathbf{b}_t(L))\Phi_t(L)^\top), \end{aligned}$$

where \mathbf{E}_p and Cov_p are the expectation and covariance with respect to the posterior distribution. We choose the number of basis functions such that the criterion $\text{PPL}(L)$ is minimized. Although the order of differences, k , is typically fixed, it can also be selected by PPL.

2.4 Properties of the shrinkage prior

This section presents theoretical properties of the prior distribution and its periphery. Their proofs are described in Appendix 2.

In Section 2.1, we formulated a prior as (1) and now investigate it in detail. Its

marginal prior of λ_t is

$$\pi(\boldsymbol{\delta}_t \mid \tau, \sigma) \propto \int_0^\infty \frac{1}{\lambda_t^L(1 + \lambda_t^2)} \exp \left\{ -\frac{1}{2\sigma^2\tau^2\lambda_t^2} \boldsymbol{\delta}_t^\top \Phi_t^\top \Phi_t \boldsymbol{\delta}_t \right\} d\lambda_t.$$

Then, notable properties of the marginal prior is given by the following proposition.

Proposition 1.

$$\begin{aligned} (i) \quad & \pi(\boldsymbol{\delta}_t \mid \tau, \sigma) \rightarrow \infty \quad \text{as} \quad \boldsymbol{\delta}_t \rightarrow \mathbf{0}. \\ (ii) \quad & \pi(\boldsymbol{\delta}_t \mid \tau, \sigma) = O \left(\|\Phi_t \boldsymbol{\delta}_t\|_2^{-L-1} \right) \end{aligned}$$

(i) implies that, for given τ, σ^2 and L , the density diverges at the origin $\boldsymbol{\delta}_t = \mathbf{0}$ like the original horseshoe prior (Carvalho et al., 2009, 2010). Conspicuously, this property strongly shrinks the trivial noises toward zero at posterior inference. On the other hand, (ii) suggests that the tail decay of the marginal prior is gentle. The random variables from the prior are expected to take large values with greater probability owing to the heavy tail. These critical features of the prior distribution contribute to handling sparsity.

Next, we consider the posterior mean deduced from the prior. For simplicity, we focus on $k = 0$. In this case, the model can be rewritten as

$$\mathbf{z}_t \equiv \mathbf{y}_{t+1} - \mathbf{y}_t \sim N(\Phi_t \boldsymbol{\delta}_t, 2\sigma^2 I_n), \quad \boldsymbol{\delta}_t \equiv \mathbf{b}_{t+1} - \mathbf{b}_t \sim N(\mathbf{0}, \sigma^2 \tau^2 \lambda_t^2 (\Phi_t^\top \Phi_t)^{-1}),$$

so that the model is defined for the observed value of difference \mathbf{z}_t .

Proposition 2. *When $k = 0$, the posterior mean of $\Phi_t \boldsymbol{\delta}$ can be represented as*

$$\mathbb{E}[\Phi_t \boldsymbol{\delta} \mid \mathbf{z}] = (\Sigma^{-1} + S_0^{-1})^{-1} \Sigma^{-1} \mathbf{z} = \{I_{n(T-1)} - \Sigma(\Sigma + S_0)^{-1}\} \mathbf{z},$$

with

$$\Sigma = \sigma^2 I_n \otimes \begin{pmatrix} 2 & 1 & & \\ 1 & \ddots & \ddots & \\ & \ddots & \ddots & 1 \\ & & 1 & 2 \end{pmatrix}, \quad S_0 = \sigma^2 \tau^2 I_n \otimes \begin{pmatrix} \lambda_1^2 & & \\ & \ddots & \\ & & \lambda_{T-1}^2 \end{pmatrix},$$

where \otimes denotes the Kronecker product. Also let \mathcal{I} denote the top left $n \times n$ block of $\{I_{n(T-1)} - \Sigma(\Sigma + S_0)^{-1}\}$, and assume $\lambda_2 = \lambda_3 = \dots = \lambda_{T-1}$. Then, we obtain

$$\mathcal{I} \rightarrow I_n, \quad \text{as} \quad \lambda_1 \rightarrow \infty.$$

This quantity shows the role of the local shrinkage parameter λ_1 and how \mathbf{z}_1 contributes to the posterior mean of $\Phi_t \boldsymbol{\delta}_1$. \mathbf{z}_1 fully influences $\Phi_t \boldsymbol{\delta}_1$. This observation indicates that the prior of λ_1 has to have considerable mass on the tail to prevent over-shrunk estimation of the large signals, known as tail robustness. The use of $C^+(0, 1)$ for λ_t is motivated by this argument.

2.5 Extension to irregular grids with application to varying-coefficient functional linear model

We here consider an extension to the proposed smoothing techniques under irregularly spaced functional data. Let $Z_{t_1}(\cdot), Z_{t_2}(\cdot), \dots, Z_{t_n}(\cdot)$ be a sequence of functional random variables indexed by t_i . This situation requires that distance information be incorporated into the model. Using the same basis expansion in Section 2.1, we introduce the following prior:

$$\mathbf{b}_{t_i+h} - \mathbf{b}_{t_i} | \lambda_{t_i}, \tau, \sigma \sim N(\mathbf{0}, h\sigma^2\tau^2\lambda_{t_i}^2(\Phi_{t_i}^\top \Phi_{t_i})^{-1}), \quad h \geq 0 \quad (2)$$

where we use the same prior for λ_t^2 . Although the prior formulation (2) corresponds to the extension under first order difference, the second order cases can also be extended to the irregular grids, following the argument given by Lindgren and Rue (2008).

The prior (2) is useful for estimating varying-coefficient functional linear model

(VCFLM). VCFLM is a combination of scalar-on-function model and varying coefficient model, that is, the coefficient is function which changes according to some exogenous variable (e.g. Matsui, 2022; Wu et al., 2010; Cardot and Sarda, 2008). The model is described as

$$y_{t_i} = \int_{\mathcal{S}} Z(t_i, s) x_{t_i}(s) ds + \varepsilon_i, \quad i = 1, \dots, n, \quad (3)$$

where $x_{t_i}(\cdot)$ is a predictor function, y_{t_i} is a scalar response, and $Z(t_i, s)$ is a coefficient function at $t_i \in \mathcal{T} \subset \mathbb{R}$. Without loss of generality, we can assume $t_1 < t_2 < \dots < t_n$. By expanding $Z(t_i, s)$ and $x_{t_i}(s)$ by orthonormal basis functions

$$Z(t_i, \cdot) = \sum_{\ell=1}^L b_{t_i \ell} \phi_{\ell}(\cdot), \quad x_{t_i}(\cdot) = \sum_{\ell=1}^L c_{t_i \ell} \phi_{\ell}(\cdot),$$

the model (3) reduces to

$$y_{t_i} = \mathbf{b}_{t_i}^{\top} \mathbf{c}_{t_i} + \varepsilon_i, \quad \varepsilon_i \sim N(0, \sigma^2), \quad i = 1, \dots, n.$$

Then we can adopt the prior (1) for \mathbf{b}_{t_i} . Since the response y_{t_i} is Gaussian, we can easily derive a similar Gibbs sampling algorithm to approximate posterior distribution of \mathbf{b}_{t_i} .

3 Simulation Studies

3.1 Simulation settings

We evaluate the performance of the proposed and existing methods through simulation studies. For $t = 1, \dots, T(= 50)$ and the domain $\mathcal{X} = [1, n]$ with $n = 120$, we prepared

the following four scenarios as the true trend function $\beta_t(x)$:

- (1) Constant: $\beta_t(x) = f_1(x)$,
- (2) Smooth: $\beta_t(x) = f_1(x) \sin \frac{t+x}{5}$,
- (3) Piecewise constant: $\beta_t(x) = \sum_{i=1}^5 f_i(x) \mathbb{I}_{\{10(i-1) < t \leq 10i\}}$,
- (4) Varying smoothness: $\beta_t(x) = f_1(x) + 20 \left\{ \sin \left(\frac{4t}{n} - 2 \right) + 2 \exp \left(-30 \left(\frac{4t}{n} - 2 \right)^2 \right) \right\}$,

where f_i ($i = 1, \dots, 5$) is a sample path of the Gaussian process associated to RBF kernel $k_i(x_1, x_2) = \theta_i^2 \exp(-\|x_1 - x_2\|^2 / 2\theta_i^2)$ with a hyper-parameter θ_i . We set $\theta_i = 30, 20, 35, 25, 30$ for $i = 1, 2, \dots, 5$.

The observed data were generated by adding noises from $N(0, 5^2)$ to trend functions at equally spaced $H = 120$ points of x , namely, $x \in \{1, 2, \dots, H\}$. Figure 1 shows how the trends change over time.

In scenario 1, we investigate whether the proposed methods are able to discover the trend is constant over time even in the presence of noise. Scenario 2 checks the ability of the methods to extract a continuous curve from noisy data. Scenario 3 reveals the ability of the methods to detect abrupt changes between intermittent straight horizons, that is, discontinuity points. In scenario 4, we examine whether the methods can capture periods when the smoothness of the trend changes significantly.

3.2 Homogeneously observed data

We first considered using the full dataset generated according to the method presented in the previous section, which we call *homogeneously observed data*. For the simulated data, we applied the following methods:

- FHS: functional horseshoe smoothing.
- FLS: an artificial alternative method using the Laplace-like prior, that is, $\lambda_t \sim \text{Exp}(1)$.
- B-spline: a curve fitting method using B-spline function, which is also used as the basis of the above two methods.

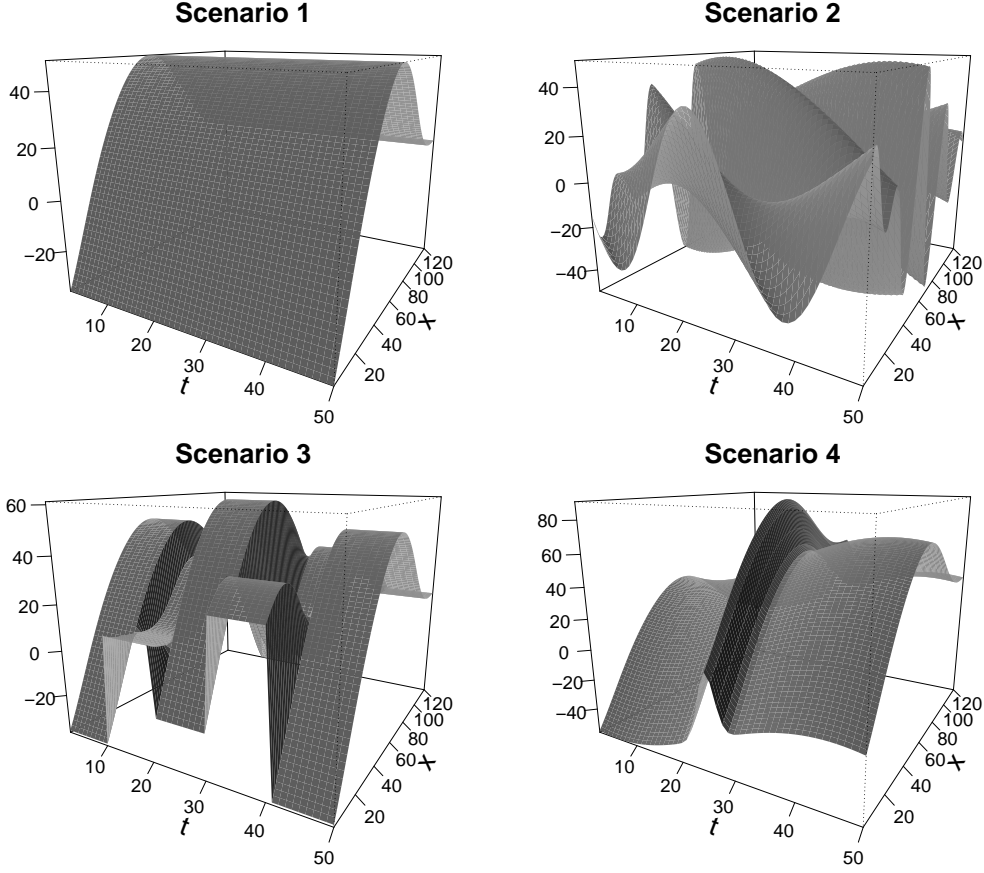


Figure 1: Each surface represents a three-dimensional plot of the true trend.

The motivation using the FLS method is to address the importance of the half-Cauchy prior for the local parameter λ_t as discussed in Section 2. For the Bayesian methods, we used 3000 posterior draws after discarding 3000 burn-in samples. In the two methods, FHS and FLS, the optimal number of the basis functions, L , and the order of difference, k , is selected via the PPL criterion among candidates $L \in \{5, 9, 13, 17, 21, 25\}$.

For the evaluation of point estimates, we adopted the following two criteria:

- Mean absolute deviation (MAD): Difference between the posterior medians and the true values, defined as

$$\text{MAD} = \frac{1}{HT} \sum_{x=1}^H \sum_{t=1}^T |\hat{\beta}_t(x) - \beta_t(x)|.$$

- Mean absolute sequentially variational deviation (MASVD): Difference of mag-

nitude of change between in the estimated trend and in the true trend, defined as

$$\text{MASVD} = \frac{1}{H(T-1)} \sum_{x=1}^H \sum_{t=1}^{T-1} |(\hat{\beta}_{t+1}(x) - \hat{\beta}_t(x)) - (\beta_{t+1}(x) - \beta_t(x))|.$$

Moreover, we used the following two criterion to evaluate 95% credible intervals obtained from FHS and FLS:

- Mean credible interval width (MCIW): The width of intervals, define as

$$\text{MCIW} = \frac{1}{HT} \sum_{x=1}^H \sum_{t=1}^T \hat{\beta}_t^{97.5}(x) - \hat{\beta}_t^{2.5}(x),$$

where $\hat{\beta}_t^{97.5}(x)$ and $\hat{\beta}_t^{2.5}(x)$ correspond to 97.5 and 2.5 percentiles of posterior distribution for $\beta_t(x)$.

- Mean coverage (MC): The coverage accuracy of the credible interval, defined as

$$\text{MC} = \frac{1}{HT} \sum_{x=1}^H \sum_{t=1}^T \mathbb{I}_{\{\hat{\beta}_t^{97.5}(x) > \beta_t(x) > \hat{\beta}_t^{2.5}(x)\}}.$$

Specifically, $k = 0$ for scenario 1 and 3, and $k = 1$ for the other scenarios. We repeated the simulations for 150 times, and the results are presented in Table 1.

Overall, we found that FHS had better performance than FLS from Table 1. The concrete discussion is as follows. First, regarding scenario 1, it can be seen that FHS had a higher ability to reduce the estimator to zero from both the figure and the table. Although FLS was not so good as FHS, it shrunk to a great extent. In scenario 3, the distinction between FHS and FLS became evident. FHS was able to estimate trend almost horizontally where the amount of change is zero and made large changes only at the discontinuous points. In contrast, FLS had less ability to make sparse estimates, resulting in a gently curved estimate. In scenario 4, there was almost no difference between FHS and FLS in the smooth part of the trend, but FHS was more accurate when the trend changes abruptly. Sudden changes and a sharp peak were captured by FHS, while FLS oversmoothed the trend where the smoothness varied significantly

Table 1: MAD (mean absolute deviation), MCIW (mean credible interval width), MASVD (mean absolute sequentially variational deviation), MC (mean coverage) and the number L of basis for FHS (the estimator using the horseshoe-like prior), FLS (the estimator based on the Laplace-like prior) and B-spline for each scenario.

Scenario	Method	MAD	MCIW	MASVD	MC	L
1	FHS	0.538	3.321	0.224	0.981	17.9
	FLS	0.673	4.374	0.314	0.990	24.9
	B-spline	1.495	-	2.112	-	17.9
	B-spline	1.127	-	0.851	-	24.9
2	FHS	0.961	5.214	0.606	0.966	23.4
	FLS	0.940	4.590	0.452	0.941	24.9
	B-spline	1.739	-	2.457	-	23.4
	B-spline	1.333	-	0.741	-	24.9
3	FHS	0.713	4.350	0.396	0.982	21.5
	FLS	3.701	6.307	2.964	0.592	9.24
	B-spline	1.560	-	2.203	-	21.5
	B-spline	4.045	-	3.440	-	9.24
4	FHS	0.814	3.988	0.529	0.937	19.0
	FLS	1.523	4.276	1.182	0.807	10.1
	B-spline	1.542	-	2.171	-	19.0
	B-spline	1.868	-	1.493	-	10.1

(where the second-order difference became large). In the data where abrupt changes did not exist, the curve could be estimated better by FLS, as the results in scenario 2 show. However, the differences were subtle, and the usefulness of FHS should not be compromised even in this situation. Those results revealed FHS to be efficient in all situations.

Next, we investigated how the credible intervals change with the sample size. We changed the number H of data at each time from 120 to 60 and compared that with the original settings with respect to MCIW and MC. According to Table 2, the more data we got, the narrower the range of CIs were, even though the MC remained almost the same. This result is consistent with the fact that uncertainty decreases with more data. This suggests that in trend estimation of functional data, not only the number of functions but also the number of observation points for each function is essential.

Furthermore, we fixed the number of basis functions fixed at 25 beforehand and implemented our method. In the literature dealing with similar models (e.g. Yang et al.,

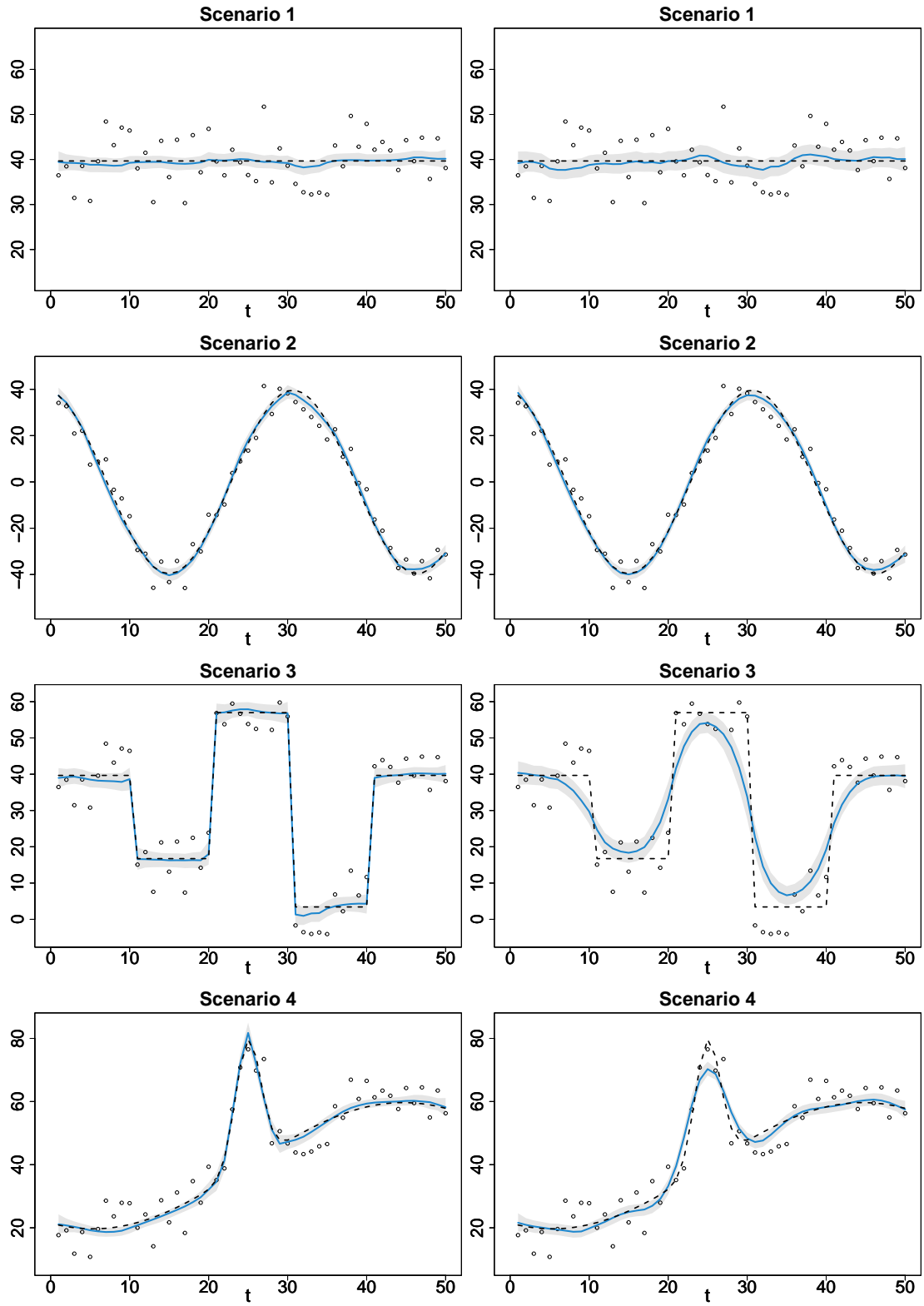


Figure 2: The dotted line is the true trend, the blue line is the estimated trend, and the gray area is the 95% point-wise CIs at $x = 40$. Of the eight figures, the four on the left are FHS, and FLS is used on the other side.

Table 2: MCIW (mean credible interval width), MASVD (mean absolute sequentially variational deviation), MC (mean coverage) of FHS with horseshoe prior for $H = 120$ and for $H = 60$.

Scenario	H	MCIW	MC
1	120	3.321	0.981
	60	4.879	0.985
2	120	5.214	0.966
	60	6.513	0.964
3	120	4.350	0.982
	60	6.234	0.979
4	120	3.988	0.937
	60	5.389	0.940

2017), the number of basis is fixed. Also, in the classical approaches (e.g. Martínez-Hernández and Genton, 2021; Kowal et al., 2019), ad hoc choices are made, such as considering cumulative explained variance. Those approach took a larger number of basis than necessary. Then we investigated whether the choice of basis is meaningful, i.e., the advantage of basis selection over preparing many basis. The results are shown in Table 3. It can be seen that, in general, the accuracy was better with the choice of basis. Hence, choosing the number of basis played an essential role in increasing the accuracy. Since this model is a fully Bayesian framework, we could use a simple selection criterion, PPL. This is one advantage in the Bayesian models.

3.3 Heterogeneously observed data

We examined the cases where 5% and 10% of the whole data were omitted at random. We report the results in Table 4 based on 3,000 MCMC iterations obtained after a burn-in period of 3,000 iterations. As the percentage of omitted data increased, the data became more unequally spaced and the estimation became less precise, but it was still able to capture the trend accurately. The wide MCIW implied the increase in uncertainty due to the omitted data. In addition, it should have been challenging to estimate where there is no data, but the Figure 3 suggests that the estimation could follow the trend including these points. This provides evidence that heterogeneity in both the number of sampling points and the sampled locations does not make implementation

Table 3: MAD (mean absolute deviation), MCIW (mean credible interval width), MASVD (mean absolute sequentially variational deviation) and MC (mean coverage) for FHS (the estimator using the horseshoe-like prior) with different number of basis for each scenario.

Scenario	Method	L	MAD	MCIW	MASVD	MC
1	selected	17.9	0.538	3.321	0.224	0.981
	fixed	25.0	0.571	3.658	0.188	0.986
2	selected	23.4	0.961	5.214	0.606	0.966
	fixed	25.0	0.981	5.362	0.609	0.967
3	selected	21.5	0.713	4.350	0.396	0.982
	fixed	25.0	0.749	4.572	0.390	0.982
4	selected	19.0	0.814	3.988	0.529	0.937
	fixed	25.0	0.896	4.361	0.545	0.935

Table 4: MAD (mean absolute deviation), MCIW (mean credible interval width), MASVD (mean absolute sequentially variational deviation) and MC (mean coverage) for FHS (the estimator based on the horseshoe-like prior) for each scenario under heterogeneously observed points.

Scenario	omitted rate	MAD	MCIW	MASVD	MC
1	0%	0.538	3.321	0.224	0.981
	5%	0.674	4.335	0.389	0.985
	10%	0.727	4.622	0.440	0.985
2	0%	0.961	5.214	0.606	0.966
	5%	1.017	5.599	0.664	0.968
	10%	1.066	5.822	0.713	0.968
3	0%	0.713	4.350	0.396	0.982
	5%	0.821	5.056	0.527	0.982
	10%	0.862	5.277	0.587	0.980
4	0%	0.814	3.988	0.529	0.937
	5%	0.889	4.784	0.632	0.964
	10%	0.889	4.806	0.674	0.964

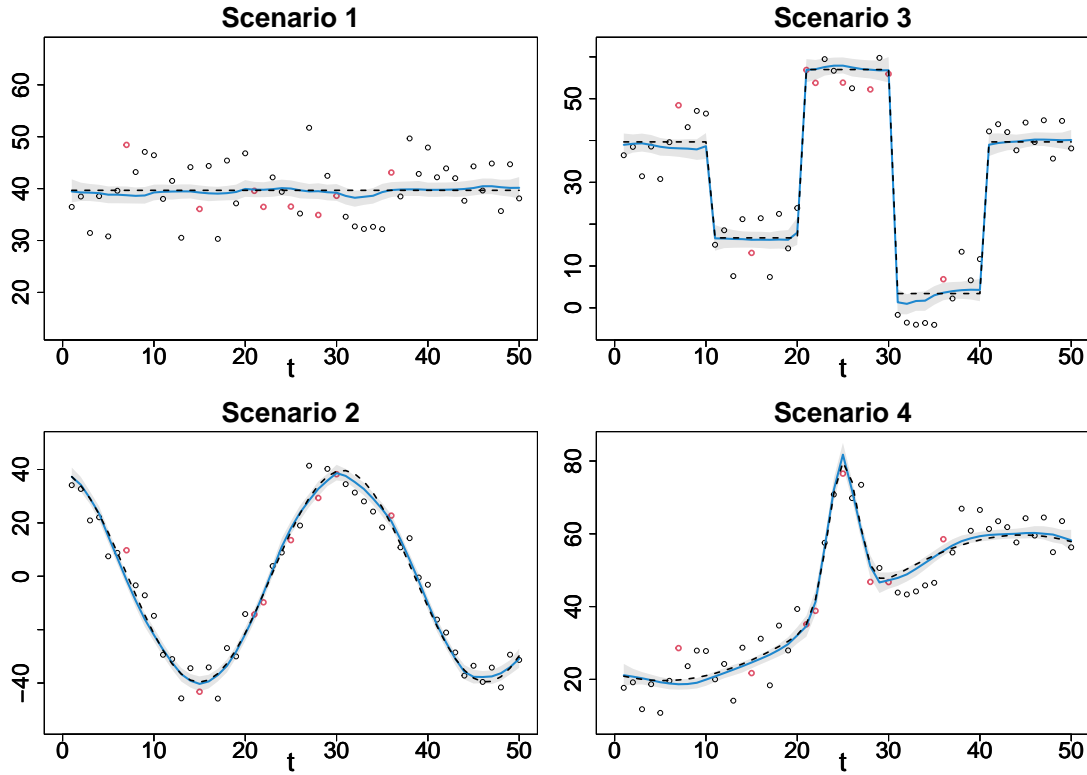


Figure 3: The dotted line is the true trend, the blue line is the estimated trend, the gray area is the 95% CIs at $x = 40$, and red dots indicate omitted measurements. The data acquisition interval is uneven, and missing values exist.

challenging or have a significant negative impact on accuracy.

4 Empirical Application

Many studies have demonstrated the applicability and performance of functional time series analysis methods using age-specific fertility data (e.g. Hyndman and Ullah, 2007; Wakayama and Sugawara, 2021). This section presents an empirical application of the proposed method using annual age-specific Australian fertility rates, which were obtained from the Australian Bureau of Statistics. These are defined as the number of births per 1,000 female residents. This data covers the age group 15 – 49 and the period 1921 – 2015. We then consider that there are 95 functions with the domain $[15, 49]$. Our interest in this application is the transition of the functions over time.

We applied functional horseshoe smoothing (FHS) and its Laplace prior version (FLS). The numbers of the basis for FHS and FLS were 27 and 20, chosen via PPL from

$\{5, 6, \dots, 30\}$. Also the difference order k was selected as 1 by PPL. The observation is shown in the upper left in Figure 4, and its surface is rugged. FLS smoothed the surface and largely removed the noise. This is also the case for FHS, where the surface was smooth and the denoising effect is confirmed. The difference is that FHS left the sharp edges intact, while FLS erased the sharp edges. This implies that the FLS reduced the signal as well as the noise and hid change points. Not doing it is the strength of FHS.

We next focus on the credible interval. Figure 5 shows the difference between the 97.5 percentile and the 2.5 percentile for each year. This is a three-dimensional representation of the size of the 95% credible region. We see that FHS had a smaller credible area than FLS and regard FHS as a more plausible model.

5 Discussion

We presented the Bayesian nonparametric smoothing method for functional time series data. This enables locally adaptive estimation by exploiting the sparsity from the shrinkage prior distributions. Simulation studies and empirical applications suggest that the method’s performance, especially with a horseshoe-like prior, is good even in the presence of sharp changes.

Indeed, we elucidated its theoretical properties. We discussed two significant issues with the shrinkage prior distribution. The first is the spike at the origin of the marginal prior, and the second is the thickness of its tail. Because of this, the estimator is expected to have ideal properties of eliminating noise and detecting abrupt changes simultaneously. We further checked the latter by proving the tail robustness of the posterior expectation, albeit only for specific cases. This is a feature that has not been discussed even with trend filtering using univariate horseshoe prior distributions (e.g. Faulkner and Minin, 2018), but our result is also the case for such models.

Functional horseshoe smoothing (FHS) has two advantages over functional trend filtering (Wakayama and Sugasawa, 2021). One is that selecting the parameters is easy. In the optimization approach, selecting parameters using K-fold cross-validation was necessary, and the computational complexity increased with the number of folds and the number of parameters’ candidates. FHS has the advantage that the PPL could be

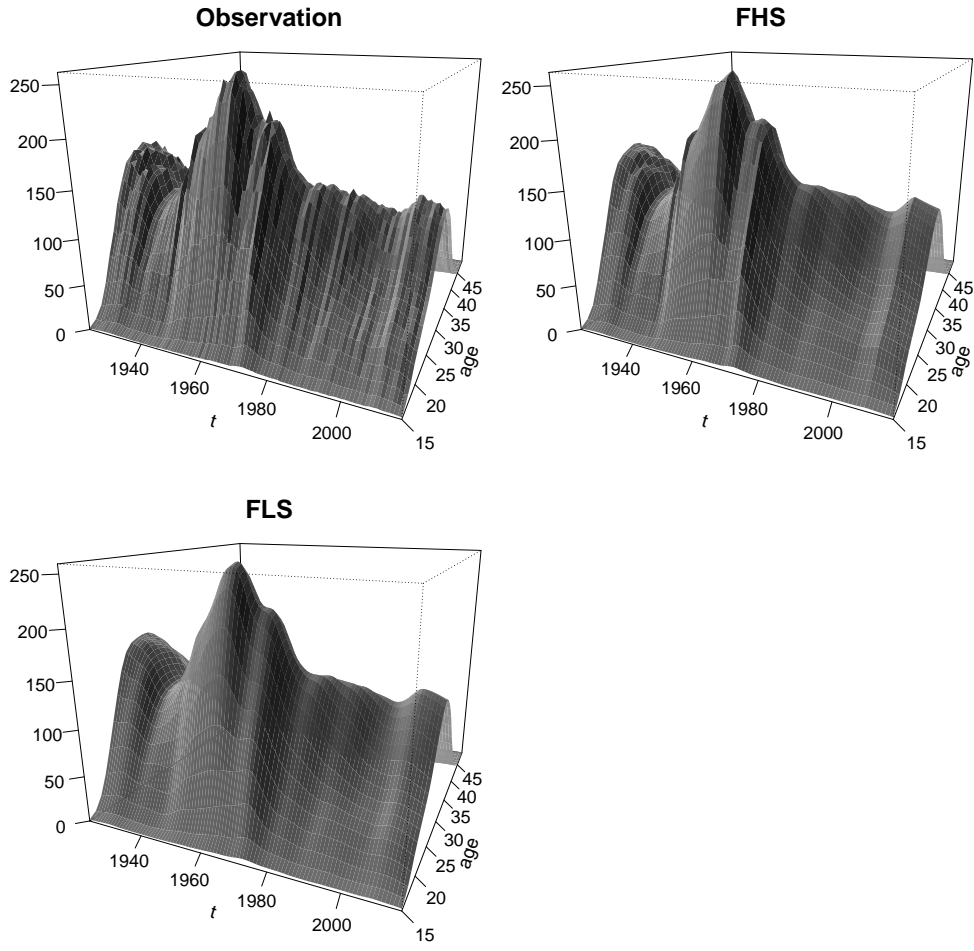


Figure 4: The number of births per 1000 female residents by age in each year in Australia. The upper left is the observed quantity and the upper right (lower left) is the smoothed surface by FHS (FLS).

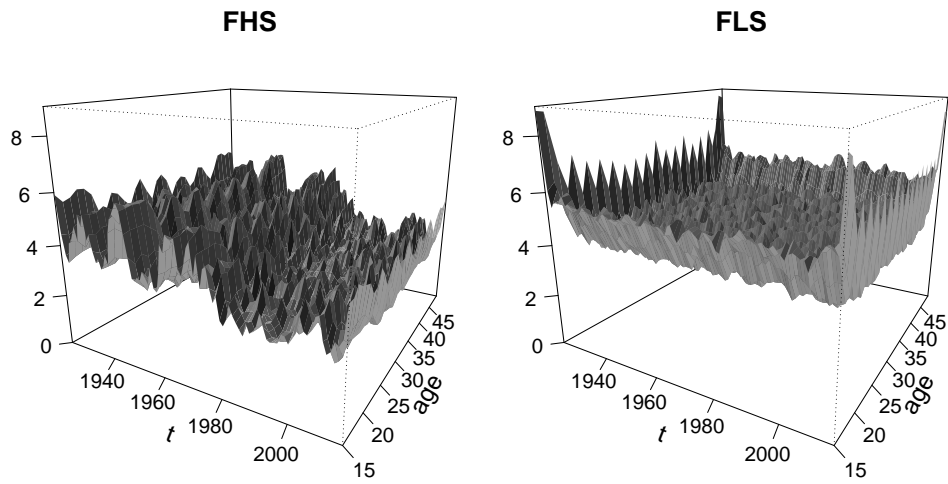


Figure 5: The left (right) figure shows the credible interval width of FHS (FLS) in three dimensions.

obtained after calculating the posterior distribution with MCMC, and the parameters could be easily selected by comparing their smallness. The other advantage is that the Bayesian model can incorporate local parameters. The optimization method uses a single parameter λ to control the overall reduction, implying that it uses only the global parameter. In other words, if a sudden change exists, the λ becomes larger to accommodate the change, and consequently, the other part becomes angular. In contrast, FHS using horseshoe-like prior allows the smooth and sharp parts of the estimation to coexist. Each part can be reduced to a different degree, owing to local parameters.

Also, FHS can deal with heterogeneously observed data. This model treats high-dimensional data as functional data, and as a result, allows heterogeneity in both the number of sampling points and the sampling locations. Hence, this model does not require missing value completion and can estimate trends without being disturbed by heterogeneity. In addition to being easy to implement, the results of simulation studies showed its good accuracy.

Appendices

Appendix 1: Detailed forms of full conditional distributions of \mathbf{b}_t

The full conditional distribution of \mathbf{b}_t is $N(\boldsymbol{\mu}_t, \Sigma_t)$. When $k = 0$, it holds that

$$\boldsymbol{\mu}_t = \begin{cases} \Sigma_t (\lambda_t^{-2} \Phi_t^\top \Phi_t \mathbf{b}_{t+1} + \lambda_{t-1}^{-2} \Phi_{t-1}^\top \Phi_{t-1} \mathbf{b}_{t-1} + \tau^2 \Phi_t^\top \mathbf{y}_t) / (\tau^2 \sigma^2) & 2 \leq t \leq T-1 \\ \Sigma_t (\lambda_t^{-2} \Phi_t^\top \Phi_t \mathbf{b}_{t+1} + \tau^2 \Phi_t^\top \mathbf{y}_t) / (\tau^2 \sigma^2) & t = 1 \\ \Sigma_t (\lambda_{t-1}^{-2} \Phi_{t-1}^\top \Phi_{t-1} \mathbf{b}_{t-1} + \tau^2 \Phi_t^\top \mathbf{y}_t) / (\tau^2 \sigma^2) & t = T \end{cases}$$

and

$$\Sigma_t^{-1} = \begin{cases} \{(\tau^2 + \lambda_t^{-2}) \Phi_t^\top \Phi_t + \lambda_{t-1}^{-2} \Phi_{t-1}^\top \Phi_{t-1}\} / (\tau^2 \sigma^2) & 2 \leq t \leq T-1 \\ (\tau^2 + \lambda_t^{-2}) \Phi_t^\top \Phi_t / (\tau^2 \sigma^2) & t = 1 \\ \tau^2 \Phi_t^\top \Phi_t + \lambda_{t-1}^{-2} \Phi_{t-1}^\top \Phi_{t-1} / (\tau^2 \sigma^2) & t = T. \end{cases}$$

Also, when $k = 1$, mean vector and precision matrix are

$$\boldsymbol{\mu}_t = \begin{cases} \Sigma_t \left(\frac{\Phi_t^\top \Phi_t (2\mathbf{b}_{t+1} - \mathbf{b}_{t+2})}{\sigma^2 \tau^2 \lambda_t^2} + \frac{\Phi_t^\top \mathbf{y}_t}{\sigma^2} \right) & t = 1 \\ \Sigma_t \left(\frac{\Phi_t^\top \Phi_t (2\mathbf{b}_{t+1} - \mathbf{b}_{t+2})}{\sigma^2 \tau^2 \lambda_t^2} + \frac{2\Phi_{t-1}^\top \Phi_{t-1} (\mathbf{b}_{t+1} + \mathbf{b}_{t-1})}{\sigma^2 \tau^2 \lambda_{t-1}^2} + \frac{\Phi_t^\top \mathbf{y}_t}{\sigma^2} \right) & t = 2 \\ \Sigma_t \left(\frac{\Phi_t^\top \Phi_t (2\mathbf{b}_{t+1} - \mathbf{b}_{t+2})}{\sigma^2 \tau^2 \lambda_t^2} + \frac{2\Phi_{t-1}^\top \Phi_{t-1} (\mathbf{b}_{t+1} + \mathbf{b}_{t-1})}{\sigma^2 \tau^2 \lambda_{t-1}^2} + \frac{\Phi_{t-2}^\top \Phi_{t-2} (2\mathbf{b}_{t-1} - \mathbf{b}_{t-2})}{\sigma^2 \tau^2 \lambda_{t-2}^2} + \frac{\Phi_t^\top \mathbf{y}_t}{\sigma^2} \right) & 3 \leq t \leq T-2 \\ \Sigma_t \left(\frac{2\Phi_{t-1}^\top \Phi_{t-1} (\mathbf{b}_{t+1} + \mathbf{b}_{t-1})}{\sigma^2 \tau^2 \lambda_{t-1}^2} + \frac{\Phi_{t-2}^\top \Phi_{t-2} (2\mathbf{b}_{t-1} - \mathbf{b}_{t-2})}{\sigma^2 \tau^2 \lambda_{t-2}^2} + \frac{\Phi_t^\top \mathbf{y}_t}{\sigma^2} \right) & t = T-1 \\ \Sigma_t \left(\frac{\Phi_{t-2}^\top \Phi_{t-2} (2\mathbf{b}_{t-1} - \mathbf{b}_{t-2})}{\sigma^2 \tau^2 \lambda_{t-2}^2} + \frac{\Phi_t^\top \mathbf{y}_t}{\sigma^2} \right) & t = T \end{cases}$$

and

$$\Sigma_t^{-1} = \begin{cases} \frac{\tau^2 \lambda_t^2 + 1}{\sigma^2 \tau^2 \lambda_t^2} \Phi_t^\top \Phi_t & t = 1 \\ \frac{\tau^2 \lambda_t^2 + 1}{\sigma^2 \tau^2 \lambda_t^2} \Phi_t^\top \Phi_t + \frac{4}{\sigma^2 \tau^2 \lambda_{t-1}^2} \Phi_{t-1}^\top \Phi_{t-1} & t = 2 \\ \frac{\tau^2 \lambda_t^2 + 1}{\sigma^2 \tau^2 \lambda_t^2} \Phi_t^\top \Phi_t + \frac{4}{\sigma^2 \tau^2 \lambda_{t-1}^2} \Phi_{t-1}^\top \Phi_{t-1} + \frac{1}{\sigma^2 \tau^2 \lambda_{t-2}^2} \Phi_{t-2}^\top \Phi_{t-2} & 3 \leq t \leq T-2 \\ \frac{\tau^2 \lambda_t^2 + 1}{\sigma^2 \tau^2 \lambda_t^2} \Phi_t^\top \Phi_t + \frac{4}{\sigma^2 \tau^2 \lambda_{t-1}^2} \Phi_{t-1}^\top \Phi_{t-1} + \frac{1}{\sigma^2 \tau^2 \lambda_{t-2}^2} \Phi_{t-2}^\top \Phi_{t-2} & t = T-1 \\ \frac{\tau^2 \lambda_t^2}{\sigma^2 \tau^2 \lambda_t^2} \Phi_t^\top \Phi_t + \frac{1}{\sigma^2 \tau^2 \lambda_{t-2}^2} \Phi_{t-2}^\top \Phi_{t-2} & t = T \end{cases}$$

Assume data is observed homogeneously, that is, $\Phi_1 = \Phi_2 = \dots = \Phi_T$. When $k = 0$, mean vector and precision matrix can be written as

$$\boldsymbol{\mu}_t = \begin{cases} \{c_t(\lambda_t^{-2} \mathbf{b}_{t+1} + \lambda_{t-1}^{-2} \mathbf{b}_{t-1}) + \tau^2 \Sigma_t \Phi^\top \mathbf{y}_t\} / (\tau^2 \sigma^2) & 2 \leq t \leq T-1 \\ (c_t \lambda_t^{-2} \mathbf{b}_{t+1} + \tau^2 \Sigma_t \Phi^\top \mathbf{y}_t) / (\tau^2 \sigma^2) & t = 1 \\ (c_t \lambda_{t-1}^{-2} \mathbf{b}_{t-1}) + \tau^2 \Sigma_t \Phi^\top \mathbf{y}_t / (\tau^2 \sigma^2) & t = T \end{cases}$$

and $\Sigma_t = c_t(\Phi^\top \Phi)^{-1}$ with

$$c_t = \begin{cases} \tau^2 \sigma^2 / (\tau^2 + \lambda_t^{-2} + \lambda_{t-1}^{-2}) & 2 \leq t \leq T-1 \\ \tau^2 \sigma^2 / (\tau^2 + \lambda_t^{-2}) & t = 1 \\ \tau^2 \sigma^2 / (\tau^2 + \lambda_{t-1}^{-2}) & t = T. \end{cases}$$

Furthermore, when $k = 1$, the forms of $\boldsymbol{\mu}_t$ and c_t are

$$\boldsymbol{\mu}_t = \begin{cases} [c_t\{(2\lambda_t^{-2} + 2\lambda_{t-1}^{-2})\mathbf{b}_{t+1} + (2\lambda_{t-1}^{-2} + 2\lambda_{t-2}^{-2})\mathbf{b}_{t-1} - \lambda_t^{-2}\mathbf{b}_{t+2} - \lambda_{t-2}^{-2}\mathbf{b}_{t-2}\} \\ \quad + \tau^2 \Sigma_t \Phi^\top \mathbf{y}_t] / (\tau^2 \sigma^2) & 3 \leq t \leq T-2 \\ [c_t(2\lambda_t^{-2}\mathbf{b}_{t+1} - \lambda_t^{-2}\mathbf{b}_{t+2}) + \tau^2 \Sigma_t \Phi^\top \mathbf{y}_t] / (\tau^2 \sigma^2) & t = 1 \\ [c_t\{(2\lambda_t^{-2} + 2\lambda_{t-1}^{-2})\mathbf{b}_{t+1} + 2\lambda_{t-1}^{-2}\mathbf{b}_{t-1} - \lambda_t^{-2}\mathbf{b}_{t+2}\} + \tau^2 \Sigma_t \Phi^\top \mathbf{y}_t] / (\tau^2 \sigma^2) & t = 2 \\ [c_t\{2\lambda_{t-1}^{-2}\mathbf{b}_{t+1} + (2\lambda_{t-1}^{-2} + 2\lambda_{t-2}^{-2})\mathbf{b}_{t-1} - \lambda_{t-2}^{-2}\mathbf{b}_{t-2}\} + \tau^2 \Sigma_t \Phi^\top \mathbf{y}_t] / (\tau^2 \sigma^2) & t = T-1 \\ [c_t(2\lambda_{t-2}^{-2}\mathbf{b}_{t-1} - \lambda_{t-2}^{-2}\mathbf{b}_{t-2}) + \tau^2 \Sigma_t \Phi^\top \mathbf{y}_t] / (\tau^2 \sigma^2) & t = T \end{cases}$$

and

$$c_t = \begin{cases} \tau^2 \sigma^2 / (\tau^2 + \lambda_t^{-2} + 4\lambda_{t-1}^{-2} + \lambda_{t-2}^{-2}) & 3 \leq t \leq T-2 \\ \tau^2 \sigma^2 / (\tau^2 + \lambda_t^{-2} + 4\lambda_{t-1}^{-2}) & t = 2 \\ \tau^2 \sigma^2 / (\tau^2 + \lambda_t^{-2}) & t = 1 \\ \tau^2 \sigma^2 / (\tau^2 + 4\lambda_{t-1}^{-2} + \lambda_{t-2}^{-2}) & t = T-1 \\ \tau^2 \sigma^2 / (\tau^2 + \lambda_{t-2}^{-2}) & t = T. \end{cases}$$

Appendix 2: Proof of the propositions

This section provides proofs of Proposition 1 and Proposition 2.

Proof of Proposition 1 (i). For $L = 1$, the divergence of $\pi(\boldsymbol{\delta}_t \mid \tau, \sigma)$ follows from the proof of Theorem 1 in Carvalho et al. (2010). We restrict our investigation to $L \geq 2$.

For simplicity, we fix $\sigma = \tau = 1$. We have

$$\begin{aligned} \pi(\boldsymbol{\delta}_t) &\propto \int_0^\infty \frac{1}{\lambda_t^L(1 + \lambda_t^2)} \exp \left\{ -\frac{1}{2\lambda_t^2} \boldsymbol{\delta}_t^\top \Phi_t^\top \Phi_t \boldsymbol{\delta}_t \right\} d\lambda_t \\ &\geq \int_0^1 \frac{1}{\lambda_t^L(1 + \lambda_t^2)} \exp \left\{ -\frac{1}{2\lambda_t^2} \boldsymbol{\delta}_t^\top \Phi_t^\top \Phi_t \boldsymbol{\delta}_t \right\} d\lambda_t. \end{aligned}$$

Let $u = \lambda_t^{-2}$. Then, we obtain

$$\begin{aligned}\pi(\boldsymbol{\delta}_t) &\geq 2 \int_1^\infty \frac{u^{\frac{L-1}{2}}}{1+u} \exp\left\{-\frac{u}{2} \boldsymbol{\delta}_t^\top \Phi_t^\top \Phi_t \boldsymbol{\delta}_t\right\} du \\ &\geq \int_1^\infty u^{\frac{L-3}{2}} \exp\left\{-\frac{u}{2} \boldsymbol{\delta}_t^\top \Phi_t^\top \Phi_t \boldsymbol{\delta}_t\right\} du.\end{aligned}$$

Also, we transform $\tilde{u} = \frac{\boldsymbol{\delta}_t^\top \Phi_t^\top \Phi_t \boldsymbol{\delta}_t}{2} u$. It leads to

$$\pi(\boldsymbol{\delta}_t) \geq \left(\frac{\sqrt{2}}{\|\Phi \boldsymbol{\delta}_t\|_2}\right)^{L-1} \int_{\frac{\|\Phi \boldsymbol{\delta}_t\|_2^2}{2}}^\infty \tilde{u}^{\frac{L-3}{2}} \exp\{-\tilde{u}\} d\tilde{u}.$$

The right-hand equals to

$$\left(\frac{\sqrt{2}}{\|\Phi \boldsymbol{\delta}_t\|_2}\right)^{L-1} \Gamma\left(\frac{L-1}{2}, \frac{\|\Phi \boldsymbol{\delta}_t\|_2^2}{2}\right),$$

where $\Gamma(\cdot, \cdot)$ is the upper incomplete gamma function. If $\boldsymbol{\delta}_t \rightarrow 0$, it holds that

$$\frac{\sqrt{2}}{\|\Phi \boldsymbol{\delta}_t\|_2} \rightarrow \infty, \quad \Gamma\left(\frac{L-1}{2}, \frac{\|\Phi \boldsymbol{\delta}_t\|_2^2}{2}\right) \rightarrow \Gamma\left(\frac{L-1}{2}\right)$$

Hence, $\pi(\boldsymbol{\delta}_t) \rightarrow \infty$ as $\boldsymbol{\delta}_t \rightarrow 0$. □

Before proving Proposition 1 (ii), we introduce an important result. First, slight modification with Lemma S5 in Hamura et al. (2020) leads to the following lemma, which gives rise to Corollary 1.

Lemma 1. *Let $f(\cdot)$ and $g(\cdot)$ be positive and continuous functions such that $e^{-\frac{1}{x}}f(x)$ and $e^{-\frac{1}{x}}g(x)$ are integrable on the real line. Then, it holds that*

$$\frac{\lim_{x \rightarrow \infty} \int_0^\infty \phi(x; 0, v) f(v) dv}{\lim_{x \rightarrow \infty} \int_0^\infty \phi(x; 0, v) g(v) dv} = \lim_{v \rightarrow \infty} \frac{f(v)}{g(v)}, \quad (4)$$

where $\phi(x; 0, v)$ is p.d.f. of $N(0, v)$.

Corollary 1. *If $\lim_{x \rightarrow \infty} f(x)/g(x) = 1$, we denote $f \approx g$. Let $f(v) = \frac{1}{v^{L/2}(1+v)}$ and $g(v) = \frac{1}{v^{L/2+1}}$ for fixed $L \in \mathbb{N}$. Then, $\int_0^\infty \phi(x; 0, v) f(v) dv \approx \int_0^\infty \phi(x; 0, v) g(v) dv$ holds.*

Proof of Corollary 1. These are obviously positive and continuous. Also $e^{-\frac{1}{x}}f(x)$ and

$e^{-\frac{1}{x}}g(x)$ are integrable on the real line, since

$$\begin{aligned}\int_0^\infty f(v)e^{-\frac{1}{v}}dv &\leq \int_0^\infty \frac{1}{v^{\frac{L}{2}+1}}e^{-\frac{1}{v}}dv + \int_0^\infty \frac{1}{v^{\frac{L}{2}}}e^{-\frac{1}{v}}dv \\ &\leq \Gamma\left(\frac{L+1}{2}\right) + \Gamma\left(\frac{L-1}{2}\right) \\ &< \infty,\end{aligned}$$

and similarly $\int_0^\infty g(v)\phi(x;0,v)dv < \infty$. Then, Lemma 1 and $\lim_{v \rightarrow \infty} f(v)/g(v) = 1$ lead to the result. \square

Based on the above results, we prove Proposition 1 (ii) as follows.

Proof of Proposition 1 (ii). For simplicity, we fix $\sigma = \tau = 1$. With transformation $\bar{u} = \lambda_t^2$,

$$\begin{aligned}\pi(\boldsymbol{\delta}_t \mid \tau, \sigma) &\propto \int_0^\infty \frac{1}{\lambda_t^L(1+\lambda_t^2)} \exp\left\{-\frac{1}{2\sigma^2\tau^2\lambda_t^2}\boldsymbol{\delta}_t^\top \Phi_t^\top \Phi_t \boldsymbol{\delta}_t\right\} d\lambda_t \\ &= \frac{1}{2} \int_0^\infty \frac{1}{\bar{u}^{\frac{L}{2}}(1+\bar{u})} \frac{1}{\bar{u}^{\frac{1}{2}}} \exp\left(-\frac{z^2}{2\bar{u}}\right) d\bar{u},\end{aligned}$$

where $z = \|\Phi_t \boldsymbol{\delta}_t\|_2$. From Corollary 1,

$$\begin{aligned}\frac{1}{2} \int_0^\infty \frac{1}{\bar{u}^{\frac{L}{2}}(1+\bar{u})} \frac{1}{\bar{u}^{\frac{1}{2}}} \exp\left(-\frac{z^2}{2\bar{u}}\right) d\bar{u} &\approx \frac{1}{2} \int_0^\infty \frac{1}{\bar{u}^{\frac{L}{2}+1}} \frac{1}{\bar{u}^{\frac{1}{2}}} \exp\left(-\frac{z^2}{2\bar{u}}\right) d\bar{u} \\ &= \frac{1}{2} \frac{\Gamma(\frac{L+1}{2})}{(\frac{z^2}{2})^{\frac{L+1}{2}}} \\ &= O(z^{-L-1}).\end{aligned}$$

\square

Next, we prove the tail robustness of the posterior mean.

Proof of Proposition 2. We consider the model

$$\mathbf{z}_t \equiv \mathbf{y}_{t+1} - \mathbf{y}_t \sim N(\Phi_t \boldsymbol{\delta}_t, 2\sigma^2 I_n), \quad \boldsymbol{\delta}_t \equiv \mathbf{b}_{t+1} - \mathbf{b}_t \sim N(\mathbf{0}, \sigma^2 \tau^2 \lambda_t^2 (\Phi_t^\top \Phi_t)^{-1}).$$

However, \mathbf{z}_t and \mathbf{z}_{t+1} are not independent since $\text{Cov}(\mathbf{z}_t, \mathbf{z}_{t+1}) = \sigma^2 I_n$. To clarify the

setting, define $\mathbf{z} = (\mathbf{z}_1^\top, \dots, \mathbf{z}_{T-1}^\top)^\top$ and $\mathbf{\Delta} = ((\Phi_t \boldsymbol{\delta}_1)^\top, \dots, (\Phi_t \boldsymbol{\delta}_{T-1})^\top)^\top$, the model is rewritten as

$$\mathbf{z} \sim N(\mathbf{\Delta}, \Sigma), \quad \mathbf{\Delta} \sim N(\mathbf{0}, S_0),$$

where

$$\Sigma = \sigma^2 I_n \otimes \begin{pmatrix} 2 & 1 & & \\ 1 & \ddots & \ddots & \\ & \ddots & \ddots & 1 \\ & & 1 & 2 \end{pmatrix}, \quad S_0 = \sigma^2 \tau^2 I_n \otimes \begin{pmatrix} \lambda_1^2 & & \\ & \ddots & \\ & & \lambda_{T-1}^2 \end{pmatrix},$$

where \otimes denotes the Kronecker product. Then, it holds that

$$\mathbb{E}[\Phi_t \boldsymbol{\delta} | \mathbf{z}] = (\Sigma^{-1} + S_0^{-1})^{-1} \Sigma^{-1} \mathbf{z} = \{I_{n(T-1)} - \Sigma(\Sigma + S_0)^{-1}\} \mathbf{z},$$

where the second equality follows from the Woodbury matrix identity. Note that $\Sigma + S_0$ is a tridiagonal matrix and its inversion is not straightforward. We here focus on the posterior mean of $\Phi_t \boldsymbol{\delta}_1$ as a function of \mathbf{z}_1 , and consider the following special case:

$$\Sigma + S_0 = \sigma^2 I_n \otimes \left(\begin{array}{c|ccc} 2 + \tau^2 \lambda_1^2 & 1 & & & \\ \hline 1 & 2 + \tau^2 \lambda_2^2 & 1 & & \\ & 1 & \ddots & \ddots & \\ & & \ddots & \ddots & 1 \\ & & & 1 & 2 + \tau^2 \lambda_2^2 \end{array} \right). \quad (5)$$

We define the first n columns of $(\Sigma + S_0)^{-1}$ as \tilde{S}_1 . Since the lower right block of the last term of (5) is tridiagonal matrix with the same diagonal entries, from the main result

of Hu and O’Connell (1996) and a general formula of block matrix inversion, we get

$$\tilde{S}_1 = \frac{1}{2 + \tau^2 \lambda_1^2 - R_{11}^{-1}} \begin{pmatrix} I_n \\ -R_{11} I_n \\ \vdots \\ -R_{1T-2} I_n \end{pmatrix},$$

where

$$R_{ij} = -\frac{\cosh(T - |j - i|)\omega - \cosh(T - j - i)\omega}{2 \sinh \omega \sinh T\omega},$$

with ω satisfying $2 \cosh \omega = 2 + \tau^2 \lambda_2^2$. Moreover, the first n rows of Σ is $(2I_n, I_n, O_n, \dots, O_n)$.

Thus, the top left $n \times n$ block of $\{I_{n(T-1)} - \Sigma(\Sigma + S_0)^{-1}\}$ is

$$\mathcal{I} = \left(1 - \frac{2 - R_{11}}{2 + \tau^2 \lambda_1^2 - R_{11}^{-1}}\right) I_n.$$

If $\lambda_1 \rightarrow \infty$, \mathcal{I} converges to I_n . □

References

- Aue, A., L. Horváth, and D. F. Pellatt (2017). Functional generalized autoregressive conditional heteroskedasticity. *Journal of Time Series Analysis* 38(1), 3–21.
- Aue, A. and J. Klepsch (2017). Estimating functional time series by moving average model fitting. *arXiv preprint arXiv:1701.00770*.
- Besse, P. C., H. Cardot, and D. B. Stephenson (2000). Autoregressive forecasting of some functional climatic variations. *Scandinavian Journal of Statistics* 27(4), 673–687.
- Bosq, D. (2000). *Linear processes in function spaces: theory and applications*, Volume 149. Springer Science & Business Media.
- Canale, A. and M. Ruggiero (2016). Bayesian nonparametric forecasting of monotonic functional time series. *Electronic Journal of Statistics* 10(2), 3265–3286.

- Cardot, H. and P. Sarda (2008). Varying-coefficient functional linear regression models. Communications in statistics—theory and methods 37(20), 3186–3203.
- Carvalho, C. M., N. G. Polson, and J. G. Scott (2009). Handling sparsity via the horseshoe. In Artificial Intelligence and Statistics, pp. 73–80. PMLR.
- Carvalho, C. M., N. G. Polson, and J. G. Scott (2010). The horseshoe estimator for sparse signals. Biometrika 97(2), 465–480.
- Cerovecki, C., C. Francq, S. Hörmann, and J.-M. Zakoian (2019). Functional garch models: the quasi-likelihood approach and its applications. Journal of econometrics 209(2), 353–375.
- Faulkner, J. R. and V. N. Minin (2018). Locally adaptive smoothing with markov random fields and shrinkage priors. Bayesian analysis 13(1), 225.
- Gao, Y., H. L. Shang, and Y. Yang (2019). High-dimensional functional time series forecasting: An application to age-specific mortality rates. Journal of Multivariate Analysis 170, 232–243.
- Gelfand, A. E. and S. K. Ghosh (1998). Model choice: a minimum posterior predictive loss approach. Biometrika 85(1), 1–11.
- Hamura, Y., K. Irie, and S. Sugawara (2020). Log-regularly varying scale mixture of normals for robust regression. arXiv preprint arXiv:2005.02800.
- Hörmann, S., L. Horváth, and R. Reeder (2013). A functional version of the arch model. Econometric Theory, 267–288.
- Hörmann, S., L. Kidziński, and M. Hallin (2015). Dynamic functional principal components. Journal of the Royal Statistical Society: Series B: Statistical Methodology, 319–348.
- Horváth, L. and P. Kokoszka (2012). Inference for functional data with applications, Volume 200. Springer Science & Business Media.

- Hu, G. and R. F. O’Connell (1996). Analytical inversion of symmetric tridiagonal matrices. Journal of Physics A: Mathematical and General 29(7), 1511.
- Hyndman, R. J. and M. S. Ullah (2007). Robust forecasting of mortality and fertility rates: a functional data approach. Computational Statistics & Data Analysis 51(10), 4942–4956.
- Kakikawa, Y., K. Shimamura, and S. Kawano (2022). Bayesian fused lasso modeling via horseshoe prior. arXiv preprint arXiv:2201.08053.
- Klepsch, J. and C. Klüppelberg (2017). An innovations algorithm for the prediction of functional linear processes. Journal of Multivariate Analysis 155, 252–271.
- Klepsch, J., C. Klüppelberg, and T. Wei (2017). Prediction of functional arma processes with an application to traffic data. Econometrics and Statistics 1, 128–149.
- Kokoszka, P. and M. Reimherr (2017). Introduction to functional data analysis. CRC press.
- Kowal, D. R., D. S. Matteson, and D. Ruppert (2019). Functional autoregression for sparsely sampled data. Journal of Business & Economic Statistics 37(1), 97–109.
- Kühnert, S. et al. (2020). Functional arch and garch models: A yule-walker approach. Electronic Journal of Statistics 14(2), 4321–4360.
- Lindgren, F. and H. Rue (2008). On the second-order random walk model for irregular locations. Scandinavian journal of statistics 35(4), 691–700.
- Makalic, E. and D. F. Schmidt (2015). A simple sampler for the horseshoe estimator. IEEE Signal Processing Letters 23(1), 179–182.
- Martínez-Hernández, I. and M. G. Genton (2021). Nonparametric trend estimation in functional time series with application to annual mortality rates. Biometrics 77(3), 866–878.
- Matsui, H. (2022). Truncated estimation for varying-coefficient functional linear model. arXiv preprint arXiv:2203.10268.

- Petris, G. (2013). A bayesian framework for functional time series analysis. arXiv preprint arXiv:1311.0098.
- Ramsay, J. O. (2004). Functional data analysis. Encyclopedia of Statistical Sciences 4.
- Shin, M., A. Bhattacharya, and V. E. Johnson (2020). Functional horseshoe priors for subspace shrinkage. Journal of the American Statistical Association 115(532), 1784–1797.
- Spangenberg, F. (2013). Strictly stationary solutions of arma equations in banach spaces. Journal of Multivariate Analysis 121, 127–138.
- Wakayama, T. and S. Sugawara (2021). Trend filtering for functional data. arXiv preprint arXiv:2104.02456.
- Wu, Y., J. Fan, and H.-G. Müller (2010). Varying-coefficient functional linear regression. Bernoulli 16(3), 730–758.
- Yang, J., D. D. Cox, J. S. Lee, P. Ren, and T. Choi (2017). Efficient bayesian hierarchical functional data analysis with basis function approximations using gaussian–wishart processes. Biometrics 73(4), 1082–1091.
- Yang, J., H. Zhu, T. Choi, and D. D. Cox (2016). Smoothing and mean–covariance estimation of functional data with a bayesian hierarchical model. Bayesian Analysis 11(3), 649–670.
- Zellner, A. (1986). On assessing prior distributions and bayesian regression analysis with g-prior distributions. Bayesian inference and decision techniques.